RSC Advances

PAPER

View Article Online
View Journal | View Issue

Open Access Article. Published on 22 January 2021. Downloaded on 12/30/2025 1:39:20 AM.
This article is licensed under a Creative Commons Attribution-NonCommercial 3.0 Unported Licence.

Check for updates

Cite this: *RSC Adv.*, 2021, **11**, 4478

An Amberlite IRA-400 Cl^- ion-exchange resin modified with *Prosopis juliflora* seeds as an efficient Pb^{2+} adsorbent: adsorption, kinetics, thermodynamics, and computational modeling studies by density functional theory†

Sivaprakasam Anbazhagan,*[a] Venugopal Thiruvengadam*[a] and Anandhakumar Sukeri[b]

A *Prosopis juliflora*-seed-modified Amberlite IRA-400 Cl^- ion-exchange resin (hereafter denoted as SMA resin) is used for the removal of Pb^{2+} from wastewater. SEM, EDX, FT-IR, BET, XRD, and XPS analyses were used to characterize the SMA resin. Parameters such as Pb^{2+} concentration, pH, temperature, and time are optimized. The obtained results show that the SMA resin has high efficiency for the removal of Pb^{2+} (73.45%) at a concentration of 100 mg L^{-1} and a dosage of 0.01 g at pH 6. Thermodynamic studies indicate that the adsorption was spontaneous with negative ΔH° and ΔS° values at all temperatures; pseudo-second-order kinetics and the Langmuir adsorption isotherm provided the best fit (q_{max} = 106 mg g^{-1} and R^2 = 0.99) from 298 to 338 K. In addition, a diffusion-controlled mechanism at 298 K was observed from intra-particle studies. A desorption and recovery process has been applied successfully to the SMA adsorbent. The obtained results showed desorption of 90.7% at pH 2.5 with 86.3% recovery over six cycles. Furthermore, the DFT results suggest that all the functional groups of the SMA resin possibly bind with Pb^{2+} and, of these, the –C=O group shows the highest binding energy towards Pb^{2+}. Moreover, the high-efficiency removal of Pb^{2+} from synthetic wastewater using the proposed SMA resin was demonstrated to show the real-life application potential.

Received 1st December 2020
Accepted 30th December 2020

DOI: 10.1039/d0ra10128a

rsc.li/rsc-advances

1. Introduction

Environmental pollution, in particular water pollution, is one of the biggest problems worldwide and it causes economic and physical damage on an everyday basis. It has been an issue of continuously increasing concern that needs to be taken care of.[1] Water pollution occurs mainly when people overload the water environment with waste. It is defined as the contamination of streams, lakes, underground water, bays, and oceans with substances that are harmful to living things.[2] Heavy metals such as lead, mercury, copper, cadmium, zinc, nickel, and chromium are the most common pollutants found in industrial effluent. Even at low concentrations, these metals can be toxic to organisms, including humans.[3] Lead is a naturally occurring metal that is found in rocks, soil, water, and air. Lead, a toxic pollutant of importance, enters the environment from various anthropogenic sources, as well as *via* natural geochemical processes. It can build up in the food chain and does not easily undergo biological degradation.[4] Lead as a poisonous metal can cause severe health problems in humans. Lead poisoning is commonly a result of the ingestion of food or water that has been contaminated with lead, or it may be caused by the accidental ingestion of contaminated soil, dust, or lead-based paint.[5] Long-term exposure to lead may cause weakness, high blood pressure, anemia, and brain and kidney damage in adults and children, it may lead to miscarriages in the case of pregnant women, and it can also affect aquatic and human systems.[6] One of the main sources of lead contamination in water streams is the discharge of industrial wastewater related to mining, electroplating, metal processing, battery manufacturing, tanneries, textile production, fertilizers, pesticides, pigments, paints, and munitions.[7,8] The main industrial sources of lead also include oil-refining industries and motor vehicles that use petrol. It

[a]*Department of Chemistry, Govt. College of Engineering, Salem-636011, Tamil Nadu, India. E-mail: venugopalt@gcesalem.edu.in; greenchemistry2020@gmail.com*

[b]*São Carlos Institute of Physics, University of São Paulo, Av. Trabalhador São-Carlense, 400 – Parque Arnold Schimidt, PO Box 369, São Carlos, CEP-13566-590, São Paulo, Brazil*

† Electronic supplementary information (ESI) available: Tables showing FT-IR spectral data, the parameters of various isotherm models for the adsorption of Pb^{2+} onto SMA resin, the adsorption capacities of various adsorbent, kinetic models of adsorption on Pb^{2+}-loaded SMA resin at various temperatures, thermodynamic parameters for the adsorption of Pb^{2+} onto SMA resin, and computational studies of the adsorption of Pb^{2+} on the SMA resin. See DOI: 10.1039/d0ra10128a

© 2021 The Author(s). Published by the Royal Society of Chemistry

Open Access Article. Published on 22 January 2021. Downloaded on 12/30/2025 1:39:20 AM. This article is licensed under a Creative Commons Attribution-NonCommercial 3.0 Unported Licence.

enters the environment as a result of both natural processes and anthropogenic activities.[9]

Therefore, the removal of lead is very important, and adsorption using activated carbon is a popular technology for treating industrial and domestic contaminated water. The utilization of plant seeds, seaweed, molds, yeasts, and other dead microbial biomass and agricultural waste materials as adsorbents has also been seen.[10] For instance, the elimination of heavy metals using cherry kernels and cashew nut shells has been recently explored.[11,12] Plant waste has been directly used as an adsorbent in adsorption studies, *e.g.*, mustard husks,[6] papaya wood,[9] and saltbush leaves.[13] Ion-exchange resins have played an exceptional role in metal recovery and separation, and they are widely used for pre-concentrating and removing heavy metal ions from wastewater.[14–16] However, efficiency and selectivity are key issues in this research area. Hence, the surface modification of ion-exchange resins is essential to improve the selectivity towards metallic ions and to increase the efficiency; this is generally achieved *via* introducing active functional groups onto the surface of the ion-exchange resin/membrane *via* complexation. For instance, an anion-exchange resin surface modified with a thin anionic poly-electrolyte layer has been used for the separation of sulfate and nitrate ions.[17] Methylene diphosphonate and ethylene diphosphonate were used for the separation of Ni^{2+}, Fe^{3+}, Cd^{2+}, and Zn^{2+} ions.[18] Resins with phosphonomethyl crosslinked with polyethyleneimine (PEI) were used for uranium recovery from seawater.[19] From this angle, here an attempt has been made to use an anion-exchange resin, *i.e.*, Amberlite IRA-400 (Cl form) for the removal of Pb^{2+} from seawater. However, we did not use such a resin to directly remove the metal ions (positively charged) from solution *via* an ion-exchange reaction. Instead, the Amberlite IRA-400 Cl^- ion-exchange resin was modified with *Prosopis juliflora* seeds and then used as an efficient Pb^{2+} adsorbent, because the resultant modified resin surface contains new functional groups (*e.g.*, C–OH, –COOH, C=C, *etc.*) that can increase the adsorption capacity for Pb^{2+} due to complexation with the corresponding oxygen-containing functional groups. As a result, the efficiency of Pb^{2+} removal can be enhanced with high selectivity.

Hence, this study focuses on investigating the adsorption performance of a PJ-seed adsorbent supported on an Amberlite IRA-400 Cl^- ion-exchange resin for the removal of Pb^{2+} from synthetic contaminated water. Surface coverage and surface modification using activated carbon and the removal of toxic Pb^{2+} were carried out using surface-modified Amberlite (SMA). An SMA ion-exchange resin modified with PJ seeds has not been used as adsorbent so far to the best of our knowledge. Therefore, the first attempt has been made in this study.

2. Experimental section

2.1 Materials

Fresh *Prosopis juliflora* seedpods were collected from areas near the city of Salem (Tamil Nadu, India), and they were air-dried for five days in a dark place without exposure to sunlight. The *Prosopis juliflora* seeds were then washed thoroughly, dried in a dark place for two more days, and then crushed to a fine size. The seeds were then powdered and sieved. Amberlite IRA-400 Cl^- (Table 1) and H_2SO_4 were both purchased from Sigma-Aldrich and used as received without further purification. Milli-Q water (18 Ω cm resistivity) was used for all the required solution preparations unless otherwise stated.

2.2 Instruments

Scanning electron microscopy coupled with energy-dispersive X-ray spectroscopy (SEM-EDS, TESCAN BRNO 62300), Fourier-transform infrared spectroscopy (FT-IR, PerkinElmer spectrophotometer), X-ray diffraction (XRD, GE Inspection Technologies, Germany), Brunauer–Emmett–Teller (BET, Quantachrome Corporation), and X-ray photoelectron spectroscopy (XPS, Thermo Fisher) studies are used in this study to find the various physical properties of the adsorbent.

2.3 Preparation of the adsorbent

10 g of a sieved sample of *Prosopis juliflora* seeds and 20 g of Amberlite-400 (Cl) were soaked in 80 mL of sulfuric acid (at a ratio of 1 : 2) for 24 h under constant stirring in a fume hood. The liquid portion was decanted carefully, and the precipitated solid was taken to a ceramic hood and heated to 160 °C in an air oven for 24 h. The temperature of the oven was increased by 5 °C every 15 min. The resulting mass was then thoroughly washed with water until the filtrate pH coincided with the pH of the distilled water used. After that, the surface-modified resin was dried at 105 °C for 1 h and then stored in a cool dry place (desiccator) for further analysis.

2.4 Preparation of lead standard solution

The lead stock solution was prepared *via* dissolving 1.5984 g of $Pb(NO_3)_2 \cdot 6H_2O$ in one liter of distilled water to obtain a 1000 mg L^{-1} concentration of Pb^{2+} ions. From the stock solution, 100 mg L^{-1} working solutions were used to perform the experiments. Fresh dilutions were used for each experiment if required. pH adjustments were carried out using either diluted HCl or NaOH.

2.5 Batch experiments

Batch studies were performed in a closed plastic container (500 mL capacity) with 100 mL of lead solutions of different concentrations, ranging from 10 mg L^{-1} to 200 mg L^{-1}, and adsorbent dosages from 0.01 to 0.1 g. The constant shaking of

Table 1 Characteristics of the Amberlite IRA-400 (Cl form) ion-exchange resin[20]

Matrix	Polystyrene divinylbenzene
Functional group	Quaternary ammonium $(NR_3)^+$
Ionic state	Cl^- form
Ion exchange capacity	2.6–3 eq. kg^{-1} of dry mass
Size	0.3–0.9 mm
Temperature	75 °C (max)

Open Access Article. Published on 22 January 2021. Downloaded on 12/30/2025 1:39:20 AM.
This article is licensed under a Creative Commons Attribution-NonCommercial 3.0 Unported Licence.

the solution was done using an orbital shaker at a rate of 150 rpm. The temperature throughout the experiment was maintained at a constant value. The samples were shaken for a specified time, and then the supernatant liquid was filtered and used for analysis. The pH of the solutions was also adjusted with 1 N HCl and 1 N NaOH.

The removal efficiency of the SMA resin was calculated as follows:

$$\text{Removal efficiency } (\%) = \frac{C_0 - C_e}{C_0} \times 100 \quad (1)$$

where C_0 and C_e are the initial and equilibrium concentrations of lead (mg L^{-1}) in water, respectively.

2.6 Analysis of lead after batch studies

Lead was analyzed using an atomic adsorption spectrophotometer (AAS) (Systronic, SL 163) with a lead hollow cathode lamp. Readings were taken 10 times and the average value was used for calculations. Standards were tested after every five samples to verify the accuracy of the instrument.

2.7 The desorption and regeneration of adsorbed Pb^{2+} ions

The desorption of Pb^{2+}-loaded SMA resin was carried out from pH 2 to 7, which was achieved by utilizing 1.0 M HCl and 1.0 M NaOH, after the saturation of the SMA resin with 100 mg L^{-1} Pb^{2+} ions. The SMA resin was washed several times with deionized distilled water to remove any excess Pb^{2+} ions. It was then treated with 100 mL of 0.1 M HCl and equilibrated by shaking for 3 h in an orbital shaker at 250 rpm and then filtered. The collected supernatant was used to analyze the metal ions. The desorption percentage was calculated using the given formula:

$$\text{Desorption } (\%) = \frac{D_m}{A_m} \times 100 \quad (2)$$

where D_m is the quantity of desorbed metal ions by the desorbing agent and A_m is the total quantity of metal ions adsorbed by the SMA resin.

3. Results and discussion

3.1 Characterization of the SMA resin and Pb^{2+} adsorption *via* SEM and EDX analysis

SEM images at different magnifications of the SMA resin before (Fig. 1a and b) and after (Fig. 1c) the adsorption of Pb^{2+} are shown in Fig. 1. From the SEM images, the particle size, surface area, and minimum pore size of the adsorbent were investigated. In general, the resin has a surface area that is minimal compared with other adsorbents.[21] The raw material of PJ seeds was used to modify the surface of the Amberlite resin, resulting in an increase in the surface area and pore size of the resin. These results can be concluded based on BET analysis. Furthermore, the EDX spectrum (Fig. 1d) clearly shows the presence of lead after the adsorption of Pb^{2+} onto the adsorbent.

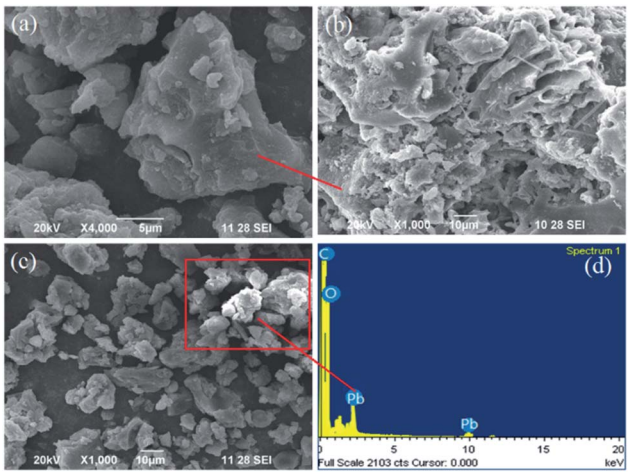

Fig. 1 SEM images of the SMA ion-exchange resin before (a and b) and after (c) Pb^{2+} adsorption. The EDX spectrum of the SMA resin after Pb^{2+} adsorption (d).

3.2 FT-IR, XRD, point of zero charge (pH_{pzc}), and textural analysis of the SMA resin

FT-IR spectra before and after the adsorption of Pb^{2+} onto the SMA resin are shown in Fig. 2a, with the corresponding adsorption band data given in Table S1.† The functional groups before the adsorption of SMA resin lead to corresponding adsorption bands at 3947.36 cm^{-1}, assigned to –NH– groups, 3420.57 cm^{-1}, assigned to –OH groups, 2928.57 cm^{-1}, assigned to C–H stretching groups, and 1599.67 cm^{-1}, 1354.98 cm^{-1}, 1040.50 cm^{-1}, and 583.93 cm^{-1}, assigned to C=O, S=O, C–X, and –C–C– functional groups, respectively.[22] Fig. 2a shows the SMA resin FT-IR spectrum after the adsorption of Pb^{2+} under the following reaction conditions: temperature, 350 °C; pH, 4; concentration, 100 mg L^{-1}; and time, 240 min. It shows some adsorption bands after the adsorption of Pb^{2+} onto the SMA resin. It can be seen that Pb^{2+} adsorption resulted in several noticeable changes (to the peaks from 1700 to 1000 cm^{-1}).

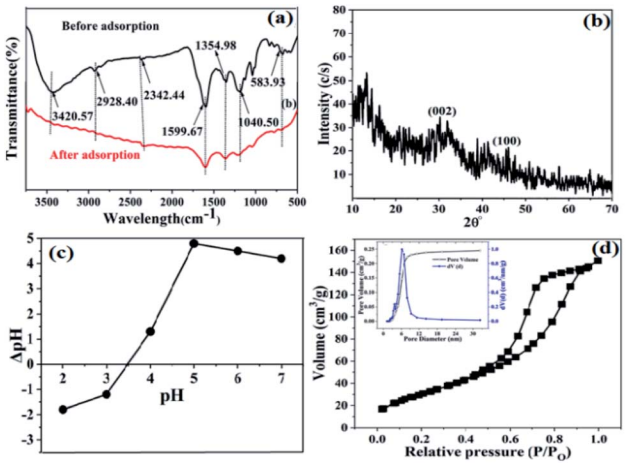

Fig. 2 The FT-IR spectra of the SMA ion-exchange resin before and after Pb^{2+} adsorption (a), the XRD pattern of the SMA resin (b), the point-of-zero-charge plot (c), and the N_2 adsorption/desorption isotherm of the SMA resin (d).

 © 2021 The Author(s). Published by the Royal Society of Chemistry

Open Access Article. Published on 22 January 2021. Downloaded on 12/30/2025 1:39:20 AM.
This article is licensed under a Creative Commons Attribution-NonCommercial 3.0 Unported Licence.

These changes (at 1610, 1358, 1213, and 1030 cm^{-1}) are owing to the attachment of Pb^{2+} ions to the surface of the adsorbent. Moreover, the amide (–NH–) peaks were widened with a reduction in intensity, shifting from 3420 to 3725.12 cm^{-1} upon the adsorption of Pb^{2+} ions onto the SMA resin. These shifts revealed that interactions between the adsorbent and adsorbate (SMA and Pb^{2+}) take place at binding or active sites on the surface of the SMA resin. Additionally, the changes suggested that complexation between Pb^{2+} and the active functional groups can also participate in the Pb^{2+} adsorption process.[23]

The XRD spectrum of the SMA resin (Fig. 2b) showed a broad diffraction peak at 2θ values between 28 and 29°, corresponding to the 002 diffraction planes of graphite.[24] No obvious diffraction pattern was noticed for the SMA resin, indicating that it was not entirely crystalline but partly amorphous. Further, the amorphous nature of the SMA resin was confirmed from the presence of broad peaks at around 28° and 44°, which can be attributed to the presence of amorphous carbon.[25] Since neither the SMA resin nor *Prosopis juliflora*-seed activated carbon are crystalline, it is not surprising that SMA does not show any crystalline nature.

Further, the solid addition method was used to investigate the pH_{pzc} value of the adsorbent. 50 mL solutions of 0.01 M $NaNO_3$ with different pH values from 2 to 12 were prepared and transferred to 100 mL beakers. Then, 0.125 g of the SMA resin was added to every beaker and they were placed for 12 h at room temperature without shaking to equilibrate. The final pH value for each adsorbent mixed solution was measured. The place where there is zero difference between the initial and final pH gives pH_{pzc} (Fig. 2c). This method was repeated 2 to 3 times using 0.01 M $NaNO_3$ solution. The point of zero charge (pH_{pzc}) value was used to find the surface charge (ionic state) and active functional groups of the adsorbent. The SMA resin adsorbent pH was neutral. The pH_{pzc} curve reveals that the SMA resin has a pH_{pzc} value of 3.5.

The BET equation was used to calculate the surface area and mean pore size and volume using the BJH (Barrett–Joyner–Halenda) method *via* N_2 adsorption/desorption at 77 K using a Quantachrome instrument. The shape obtained upon plotting the relative pressure *versus* the volume of the gas adsorbed indicates that SMA shows a type-IV adsorption isotherm as per IUPAC classifications. As can be seen in Fig. 2d, at a high relative pressure the hysteresis loop was wider, which implies that SMA has a mixed mesoporous and microporous structure. The total surface area of the SMA resin was found to be 638 $m^2\ g^{-1}$ and the existence of large mesopores compared to micropores suggests the better adsorption capacity of SMA. A higher pore size distribution in SMA indicates that the total pore volume available for Pb^{2+} was higher, resulting in a higher adsorption capacity.

3.3 X-ray photoelectron spectroscopy analysis

Fig. 3a–c shows the XPS investigation of the SMA resin. SMA shows three peaks in the XPS spectrum, corresponding to C 1s, O 1s, and N 1s peaks. The C 1s peak is a symmetrical peak in the range of ~284 to ~288 eV. This chemical shift toward a higher binding energy indicates that there are some carbon-based functional groups present on the SMA resin surface. A major aromatic carbon peak from C–C and C–H of graphitic origin is seen at around 284 eV (Fig. 3a). The peaks occurring at ~286.2 eV and ~287.3 eV can be attributed to the presence of carbon functional groups, such as C=O ether/hydroxyl, C=N, and COOH.[26] The O 1s (Fig. 3b) spectrum of SMA indicates the presence of C=O groups with a binding energy of around 531.1 eV, which may be due to ketone, aldehyde, and lactose groups. The peak at ~533.3 eV indicates the presence of C–O groups from esters, amides, or any other carboxylic acid derivatives.[27] The N 1s spectrum shows the presence of quaternary ammonium salts at around 403.0 eV due to Amberlite resin.[28] The N 1s spectrum (Fig. 3c) thus indicates that a fraction of the Amberlite resin functional groups were present on the surface of SMA.

3.4 Optimization for the removal of Pb^{2+}

(i) Effects of concentration. Fig. 4a shows the removal efficiency of the SMA ion-exchange resin using various initial concentrations of Pb^{2+} ions from 10 mg L^{-1} to 800 mg L^{-1} (at pH = 6, with an agitation time of 240 min and 0.1 g of SMA ion-exchange resin at room temperature). The removal efficiency of the SMA resin decreased with an increase in the Pb^{2+} concentration up to 100 mg L^{-1} (from 95% at 10 mg L^{-1} to 73.45% at 100 mg L^{-1}). Also, with a further increase in concentration, there was a steep decrease in the removal percentage, with higher concentrations showing lower removal percentages (about 30% at 800 mg L^{-1}). Although the removal percentage decreases at higher concentrations, the removal per gram of adsorbent increases from 95.2 mg g^{-1} (at 10 mg L^{-1}) to 240 mg g^{-1} (at 800 mg L^{-1}), which indicates that the mass of Pb^{2+} adsorbed remains the same. Further, the equilibrium of adsorption shifts towards adsorption rather than desorption with an increase in the adsorbate concentration.

(ii) Effects of time. Fig. 4b shows the effects of time on Pb^{2+} removal at different concentrations of Pb^{2+}. From this study, the total time for the removal of Pb^{2+} can be fixed at 240 min. As can be seen, high and low percentage removals were observed at low and high concentrations, respectively, with a fixed experimental

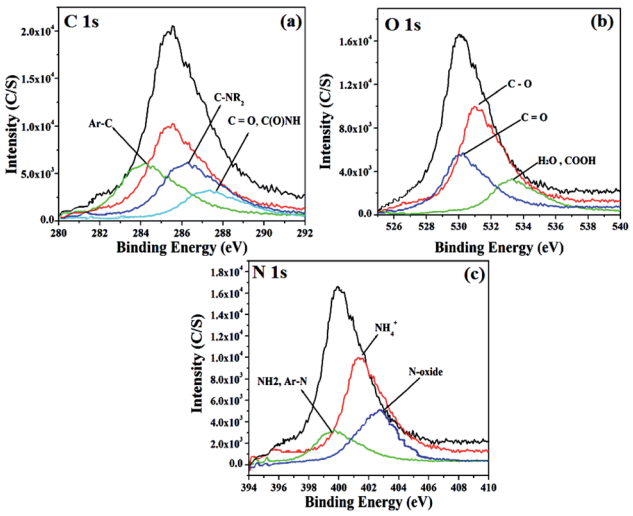

Fig. 3 XPS spectra of the SMA resin: (a) C 1s; (b) O 1s; and (c) N 1s.

Open Access Article. Published on 22 January 2021. Downloaded on 12/30/2025 1:39:20 AM.
This article is licensed under a Creative Commons Attribution-NonCommercial 3.0 Unported Licence.

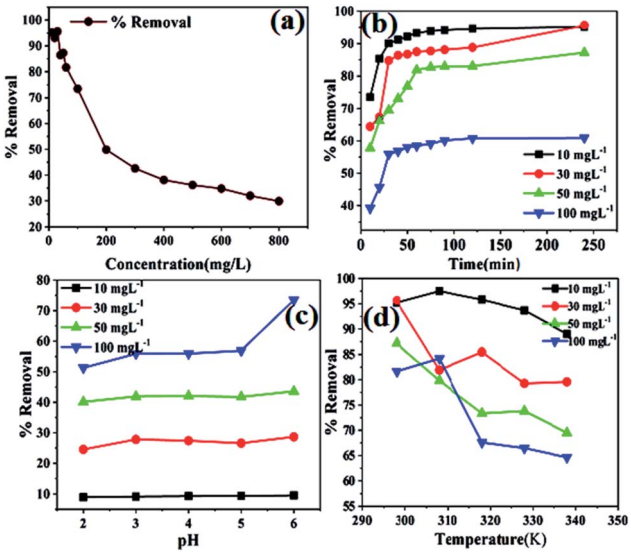

Fig. 4 The removal efficiencies *versus* Pb^{2+} concentrations using the SMA resin (10 mg L^{-1} to 800 mg L^{-1} at pH = 6, agitation time: 240 min) (a). The removal efficiencies using the SMA resin at various concentrations with increasing agitation time (b), pH (c), and temperature (d) (10 mg L^{-1} to 100 mg L^{-1}, dosage = 0.01 g, pH = 6, agitation time = 240 min).

time of 240 min. It can be reasoned that the adsorption of Pb^{2+} is more favorable on the surface of the resin at a low concentration level, whereas such processes are limited at higher concentrations due to adsorption competition. Moreover, at all concentrations the saturation limit occurs at around 100 min. With an increase in time beyond 100 min, any increases in percentage removal were negligibly small. This trend is common for adsorption by an adsorbent; initially the surface area of the adsorbent is available but with an increase in time, the number of adsorption sites decreases and saturation occurs after a certain time. The saturation time depends on the nature of adsorption (physical/chemical), the nature of the adsorbate, and the temperature. Chemical adsorption requires a long time for saturation compared with physical adsorption. A large adsorbent surface area means less time for saturation, whereas an adsorbent with a coarse nature requires a longer time for saturation. A highly polar adsorbate shows a decreased saturation time.[29]

(iii) Effects of pH. Fig. 4c shows the percentage removal of Pb^{2+} at different pH values (four different concentrations, *viz.*, 10, 30, 50, and 100 mg L^{-1}, were used for the pH studies). As can be seen, there are no appreciable changes in the adsorption capacity with an increase in the pH of the solution at 10 mg L^{-1}. Variations in adsorption with pH were quite visible at 100 mg L^{-1}, indicating an increase in adsorption with an increase in pH (pH 2 to 6). At lower pH there is competition between protons and Pb^{2+} ions for adsorption on the SMA resin, and this can affect the percentage removal due to the lower availability of adsorption sites. However, at higher concentrations, the percentage removal of Pb^{2+} increases because of the greater relative availability of adsorption sites. The removal efficiency does not effectively change with pH at most concentrations, whereas increasing the concentration significantly improves the removal efficiency. The obtained results suggest that concentration plays a more crucial role than pH. The percentage removal of Pb^{2+} increased upon increasing the pH from 2 to 6 at 100 mg L^{-1} because of the availability of more vacant active sites for adsorption. Nevertheless, at higher pH values (>8), Pb^{2+} was precipitated as $Pb(OH)_2$.[30]

(iv) Effects of temperature. Fig. 4d shows the percentage removal of Pb^{2+} with an increase in temperature at different concentrations. Five temperatures, *viz.*, 298, 308, 318, 328, and 338 K, were selected for studying the effects of temperature on the removal of Pb^{2+} ions by the SMA resin. The removal of Pb^{2+} decreases at all concentrations with an increase in temperature (Fig. 4d). However, the trend was not uniform at certain temperatures because some concentrations showed increased and decreased removal percentages with an increase in temperature and concentration. It can be reasoned that there is competition between physical and chemical adsorption.[31] It is well known that physical adsorption decreases with an increase in temperature while chemical adsorption increases. Hence, the trends in the adsorption of Pb^{2+} with an increase in temperature were not steady.

(iii) Effects of dosage. The effects of the adsorbent dose on the adsorption of lead are exhibited in Fig. 5. From the figure, it can be observed that the percentage of adsorbed Pb^{2+} increased (60.92 to 96.09%) upon increasing the adsorbent dosage from 0.1 to 1.0 g at a fixed concentration (100 mg L^{-1}) due to the availability of more active or binding sites. Moreover, after a further increase in the adsorbent dose beyond 0.1 g, no significant changes were observed in the removal percentage of Pb^{2+} ions.

3.5 Adsorption isotherm studies

Adsorption isotherms are useful for describing the distribution of the adsorbate when equilibrium is reached between the adsorbent and solution. Several isotherm models, like Langmuir, Freundlich, Dubinin–Radushkevich (DR), Temkin, and Koble–Corrigan (KC), have been reported in the literature for studying the equilibrium process.[32] Among these, suitable isotherm models can be found based on the correlation coefficient (R^2) values.

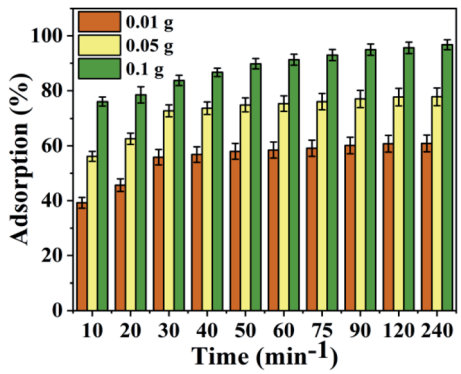

Fig. 5 The effects of SMA resin dosage on the adsorption of Pb^{2+} ions (100 mg L^{-1} at pH = 6, dosage = 0.01 to 0.1 g, agitation time = 240 min, temperature = 298 K).

 © 2021 The Author(s). Published by the Royal Society of Chemistry

Open Access Article. Published on 22 January 2021. Downloaded on 12/30/2025 1:39:20 AM.
This article is licensed under a Creative Commons Attribution-NonCommercial 3.0 Unported Licence.

(i) The Langmuir isotherm model. The Langmuir isotherm model assumes that the adsorbent surfaces are homogeneous, that binding at different sites on the adsorbent involves the same energy, and that there are no interactions between adsorbate molecules. The Langmuir isotherm model can be expressed *via* the following equation:

$$\frac{C_e}{q_e} = \frac{C_e}{q_m} + \frac{1}{q_m K_L} \tag{3}$$

where C_e (mg L^{-1}) and q_e (mg g^{-1}) are the equilibrium concentrations of lead in solution and the adsorbent under equilibrium conditions, respectively, K_L (L g^{-1}) is the Langmuir adsorption constant, and q_{max} is the monolayer adsorption capacity. Plots of C_e/q_e *vs.* C_e were used to calculate the Langmuir parameters (q_{max} and K_L), as shown in Fig. 6a, and the R^2 values are given in Table S2.† From Table S2,† the average R^2 value of 0.990 from 298 to 338 K indicates the monolayer adsorption of lead onto the SMA resin surface. Langmuir parameters like q_{max} and K_L were calculated *via* the linear regression method, which revealed that the highest R^2 value could be obtained using the Langmuir model within the studied temperature range. The q_{max} value was found to be highest at 298 K, with a value of 106.5 mg g^{-1}. Based on the existing literature, the q_{max} value of SMA resin is much better than other adsorbents, like Amberlite 400 Cl form (32.49 mg g^{-1}), hazelnut husk (13.05 mg g^{-1}),[33] tamarind wood (43.8 mg g^{-1}),[34] cellulose-modified bone char (89.9 mg g^{-1}),[35] palm-oil mill effluent (94.34 mg g^{-1}),[36] polyaniline-coated PJ seeds (90.91 mg g^{-1}),[37] ARASA (270.2 mg g^{-1}),[38] modified Aloji clay (142.57 mg g^{-1}),[39] and sludge-based bio-char (16.70 and 49.47 mg g^{-1}).[40] The q_{max} value decreases with an increase in temperature up to 328 K, but there is a value of 105.6 mg g^{-1} at 338 K, showing a sudden increase at that temperature. This trend may be attributed to the fact that an increase in temperature leads to chemisorption taking place, leading to the formation of covalent bonds between the SMA resin and Pb^{2+} ions.

(ii) The Freundlich model. The Freundlich isotherm model assumes that all adsorbent sites are not equal and that heterogeneity exists in the adsorption of the metal on the adsorbent. The Freundlich isotherm model also assumes that adsorption depends on the concentration of metal ions present in the solution. The linear form of the Freundlich isotherm model is given as:

$$\ln q_e = \ln K_F + \frac{1}{n} \ln C_e \tag{4}$$

where K_F (mg g^{-1}) represents the Freundlich adsorption constant, which gives the adsorption capacity, and n indicates the distribution of bonds between the metal and the resin, which gives the heterogeneity factor. Plots of ln q_e *vs.* ln C_e were used to find K_f and n, as shown in Fig. 6b, and the values are given in Table S2.† It was found that the values of R^2 at all temperatures were lower than the Langmuir isotherm model R^2 values. The K_f values were found to be low, indicating that the heterogeneity of adsorption was negligible, and there was no definite trend in the changes of the K_f values with an increase in temperature. Also, the value of n indicates that the heterogeneity of the adsorbent was low. The values of n (<1) and the slopes of the adsorption isotherms (>1) show that there was cooperative adsorption between Pb^{2+} and the SMA resin.

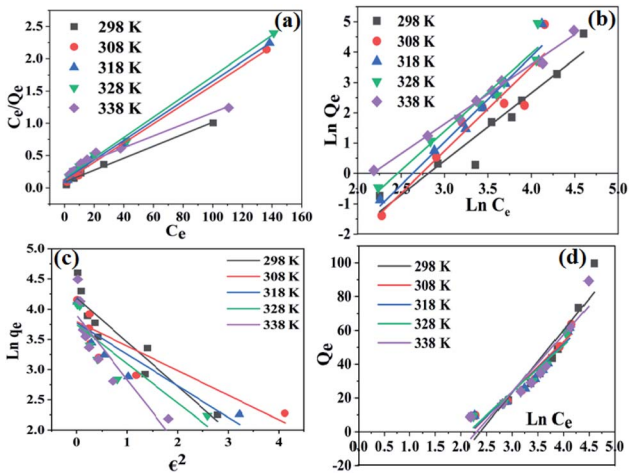

Fig. 6 Langmuir isotherm (a), Freundlich isotherm (b), Dubinin–Radushkevich isotherm (c), and Temkin isotherm (d) plots (at 100 mg L^{-1}, pH = 6, dosage = 0.01 g, agitation time = 240 min) using the Pb^{2+}-loaded SMA resin.

(iii) The Koble–Corrigan isotherm model. Both Freundlich isotherm and Langmuir isotherm characteristics are included in the Koble–Corrigan isotherm model. It is a three-parameter isotherm model and is represented as:

$$q_e = \frac{A C_e^{\,n}}{1 + B C_e^{\,n}} \tag{5}$$

where A, B, and n are the Koble–Corrigan parameters. The Koble–Corrigan parameters were found from linear plots of eqn (5), made using SciDavis 1.22 software:

$$\frac{1}{q_e} = \frac{1}{A C_e^{\,n}} + \frac{B}{A} \tag{6}$$

The values of A, B, and n were determined from the slopes and intercepts and are given in Table S2.† From Table S2,† it can be inferred that the Koble–Corrigan isotherm at 333 K showed a poor R^2 value, confirming the fact that at high temperature the mechanism of the adsorption is different from that at low temperature. The value of A was found to decrease with an increase in temperature, except at 333 K, indicating that the physical adsorption process was spontaneous at these temperatures.

(iv) The Dubinin–Radushkevich isotherm model. An equation to test the degree of rectangularity of the adsorption process is given *via* the Dubinin–Radushkevich (DR) model:

$$q_e = q_s e^{-B\varepsilon^2} \tag{7}$$

$$\varepsilon = RT \ln\left[1 + \frac{1}{C_e}\right] \tag{8}$$

where q_s corresponds to the DR adsorption capacity in mg g^{-1}, and the constant B can be related to the free energy change E (kJ

Open Access Article. Published on 22 January 2021. Downloaded on 12/30/2025 1:39:20 AM.
This article is licensed under a Creative Commons Attribution-NonCommercial 3.0 Unported Licence.

mol^{-1}) accompanying the adsorption of one Pb^{2+} ion to an adsorbent molecule *via*:

$$E = \frac{1}{\sqrt{2B}} \tag{9}$$

Plots of ln q_e *vs.* ε^2 (Fig. 6c) were used to find the values of q_s and E, and the values are presented in Table S2.† The R^2 values for the plots were found to be smaller compared to the other models. The adsorption of Pb^{2+} ions onto the SMA resin did not follow the DR model. With an increase in temperature, there was no definite trend in E and q_s. The value of E provides evidence of whether the adsorption process is chemical or physical in nature.[38] When the value of E is less than 8 kJ mol^{-1} then adsorption is predominantly physical, and when E is above 8 kJ mol^{-1} the adsorption is considered to be chemical in nature.[39] From Table S2,† it can be seen that the value of E was very low up to 328 K, which indicates physical adsorption; but at 338 K, the value of E was found to be approximately 8 kJ mol^{-1}, indicating that the adsorption mechanism was chemical in nature.[40]

(v) The Temkin isotherm model. The Temkin isotherm model is based on the generalized concept that the energy released during the adsorption process decreases with an increase in the surface coverage of the adsorbent. The Temkin isotherm model is expressed as:

$$q_e = \frac{RT}{b} \ln AC_e \tag{10}$$

Taking $RT/b = K$, the linear form of the equation is represented as:

$$q_e = K \ln A + K \ln C_e \tag{11}$$

Plots of ln C_e *vs.* q_e (Fig. 6d) were used to find K and A. In the above equation, R is the universal gas constant, and b (kJ mol^{-1}) and A (L g^{-1}) are Temkin isotherm constants. b is related to the heat of adsorption between the resin and Pb^{2+} ions. Table S2† gives the values of the Temkin constants, and it can be inferred that the correlation of the experimental data with the Temkin model was poor within the studied temperature range (298 to 308 K).

3.6 Kinetic adsorption models

The kinetics of the adsorption of Pb^{2+} ions on the SMA resin were studied to find the rate of the reaction, the rate-limiting step, and the mechanism of the process. Kinetic modeling experiments are important for gaining insight into the interactions that occur between the adsorbate and adsorbent. In this study, pseudo-first-order, pseudo-second-order, and first-order models were considered to determine the mechanism of adsorption.[41,42] For determining the kinetic parameters, 10 mL of 100 mg L^{-1} Pb^{2+}-ion solution was shaken at 250 rpm with 0.01 g of the resin for different time intervals.

(i) Pseudo-first-order model. The Lagergren model for a pseudo first-order equation was used to fit the experimental data. The linear equation is given as:

$$\ln(q_e - q_t) = \ln q_e - k_1 t \tag{12}$$

where q_t is the amount of Pb^{2+} ions absorbed at time t, and k_1 is the rate constant in min^{-1}.

Linear plots of $\ln(q_e - q_t)$ *vs.* t at various temperatures are shown in Fig. 7a. The rate constant, q_e, and R^2 values for the above plots at various temperatures are given in Table S3.† From Table S3,† the R^2 values at all temperature are found to be greater than 0.94, and the value decreases with an increase in temperature; however, q_e does not show a regular decreasing or increasing trend. The value of q_e was found to be highest at 338 K.

(ii) Pseudo-second-order model. The differential equation for the pseudo-second-order kinetics model is given as:

$$\frac{dq}{dt} = K_2(q_e - q_t)^2 \tag{13}$$

The integrated form of the equation is given as:

$$q_t = K_{id}\sqrt{t} + I \tag{14}$$

The linear form of the above equation can be represented as:

$$\frac{t}{q_t} = \frac{t}{q_e} + \frac{1}{K_2 q_e^2} \tag{15}$$

Plots of t/q_t *vs.* t at different temperatures are shown in Fig. 7b, and the intercepts and slopes of the plots are used to find the values of q_e and k_2, which are presented in Table S3.† It was found that the R^2 values at all temperatures were above 0.99, indicating that the adsorption of Pb^{2+} ions onto the resin follows a pseudo-second-order reaction. From Table S3,† it can also be inferred that the Δq values were lower than the other kinetics models.

(iii) First-order model. The first-order model was studied using the following equation:

$$\frac{1}{q_t} = \frac{k_1}{q_e t} + \frac{1}{q_e} \tag{16}$$

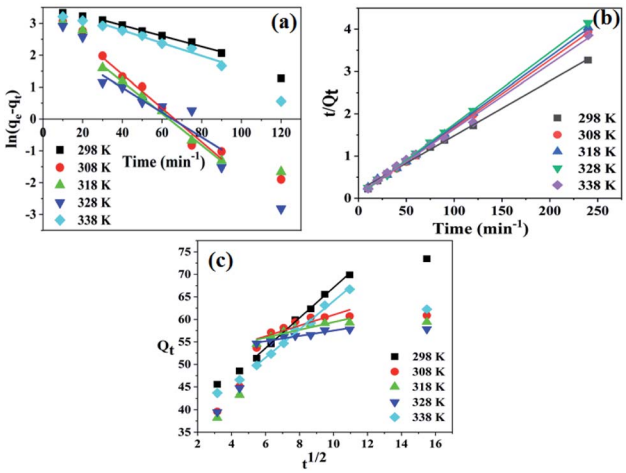

Fig. 7 Pseudo-first-order (a), pseudo-second-order (b), and intra-particle diffusion (c) model plots (at 100 mg L^{-1}, pH = 6, dosage = 0.01 g, agitation time = 240 min) using the Pb^{2+}-loaded SMA resin.

 © 2021 The Author(s). Published by the Royal Society of Chemistry

Open Access Article. Published on 22 January 2021. Downloaded on 12/30/2025 1:39:20 AM.
This article is licensed under a Creative Commons Attribution-NonCommercial 3.0 Unported Licence.

Plots of $1/q_t$ *vs.* $1/t$ (not shown) were used to calculate the values of q_e and k_1, and the values are given in Table S3.† The R^2 values for the first-order kinetics model were found to be less than 0.7, indicating that this model had the worst fit for the adsorption of Pb^{2+} ions onto the resin.

(iv) Intra-particle diffusion modeling. The intra-particle diffusion model was developed by Weber and Morris to determine whether the adsorption process involves intra-particle diffusion into the pores of the adsorbent. The linear form of the Weber and Morris equation[43] is given as:

$$q_t = K_{id}\sqrt{t} + I \tag{17}$$

Plots of q_t *vs.* $\sqrt{t}$ are given in Fig. 7c, and the Weber-and-Morris equation parameters are given in Table S4,† where I is the Weber-and-Morris constant, which is determined by the intercept, and k_{id} is the intra-particle diffusion rate constant in mg g^{-1} $min^{-1/2}$. The I and K_{id} values can be used to find the thickness of the boundary layer. If the value of I is high, subsequently, the boundary layer is considered to be thick and intra-particle diffusion is found to be more difficult.[42,43] The R^2 values in Table S4† indicate that, except at 298 K, the values of R^2 are less than 0.75. Since the R^2 values were less than 0.75, plots of q_t *vs.* $\sqrt{t}$ do not give straight lines and do not pass through the origin; therefore, the process can be considered to follow some other mechanism in addition to intra-particle diffusion. The data indicate that at a lower temperature (at 298 K), intra-particle diffusion was found to control the mechanism, whereas as the temperature increased, boundary layer accumulation seems to control the mechanism.

3.7 Thermodynamic studies

Thermodynamic parameters can give important insight into the adsorption process. A negative ΔG° value indicates that the adsorption process is spontaneous, and a highly negative value indicates that chemical adsorption is favorable.[44] The equilibrium constant K is determined using the equation:

$$K_c = \frac{q_e}{C_e} \tag{18}$$

where K_c is the equilibrium constant for the adsorption process.

ΔG°, the Gibbs free energy, was determined using the equation:

$$\Delta G^\circ = -RT \ln K_c \tag{19}$$

where R is the universal gas constant (0.008314 kJ mol^{-1} K^{-1}) and T is the absolute temperature in Kelvin.

The entropy and enthalpy changes during the adsorption process are given by the equation:

$$\Delta G^\circ = \Delta H^\circ - T\Delta S^\circ \tag{20}$$

Substituting the value from eqn (19) for ΔG° and rearranging,[42,44] we get:

$$\ln K_c = \frac{\Delta S^\circ}{R} - \frac{\Delta H^\circ}{R}\frac{1}{T} \tag{21}$$

A van't Hoff plot of ln K_c *vs.* $1/T$ (Fig. 8) was used to find ΔS° and ΔH° from the intercept and the slope, respectively, and the values are given in Table S4.† From Table S4,† it can be inferred that the ΔG° values were negative at all temperatures, indicating that the adsorption process can be considered as spontaneous. The low values of ΔG° indicate that the adsorption process was mostly physical in nature. With an increase in temperature, it was found that ΔG° decreases, indicating that the process becomes less spontaneous.[45] However, at 333 K, the ΔG° value increases, indicating a change in the mechanism at high temperature. The ΔH° value of −10.13 kJ mol^{-1} indicates that the adsorption process was energetically exothermic and feasible. However, the value of ΔS° was found to be −24.45 J mol^{-1} K^{-1}. The negative value of ΔS° indicates that the disorder decreases during the adsorption process. This trend in ΔS° can be explained *via* considering that during the adsorption process the functional group was bound to a lead ion and, hence, the rotational and vibrational energies were decreased due to this process and the resin obtained an ordered arrangement; hence, a decrease in entropy was seen.

3.8 Mechanism of adsorption/desorption

The mechanism of lead adsorption and desorption strongly depends upon the pH value of the solution on the adsorbent surface. Outlining the mechanism of any adsorption and desorption process is an essential part of understanding the methodology and explaining the physical appearance of an adsorbent; this is useful for finding out facts about a new adsorbent for future applications. A mechanism for the adsorption of Pb^{2+} ions by SMA can be explained based on the electrostatic force of attraction between the positively charged Pb^{2+} ions and the oppositely charged SMA, as shown in Fig. 9. This can be furthermore explained based on pH_{pzc}. The pH_{pzc} value of SMA was found to be 3.5. The point-of-zero-charge for an identified adsorbent surface is the pH at which that surface has a net neutral charge. The pH_{pzc} value of the adsorbent demonstrates that the external surface of the adsorbent was positively charged at a pH level lower than 3.5 and negatively charged at a pH level above 3.5. The highest level of adsorption

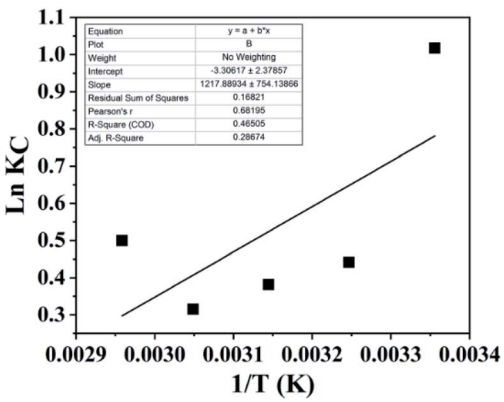

Fig. 8 A van't Hoff plot of ln K_c *vs.* $1/T$ for Pb^{2+}-ion adsorption on the SMA resin.

Open Access Article. Published on 22 January 2021. Downloaded on 12/30/2025 1:39:20 AM.
This article is licensed under a Creative Commons Attribution-NonCommercial 3.0 Unported Licence.

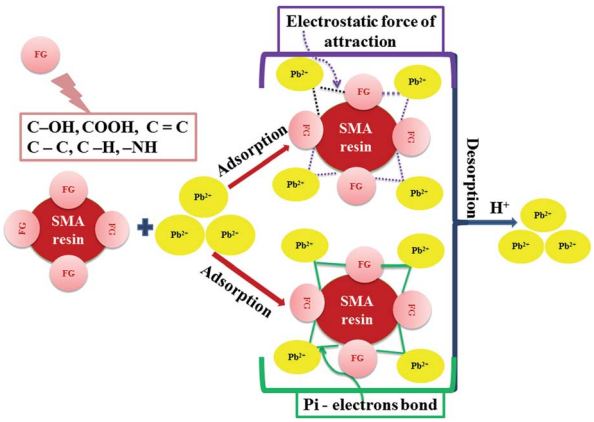

Fig. 9 The SMA-resin adsorption and desorption mechanism.

of Pb^{2+} ions on SMA occurs at pH 6, since this pH is higher than pH_{pzc}; therefore, the surface of the adsorbent is negatively charged and the quantity of H_3O^+ ions is reduced. Hence, the positively charged Pb^{2+} ions are adsorbed onto the SMA surface through electrostatic forces of attraction. Furthermore, the SMA resin has a high surface area and also many binding or active sites, which promote complexation between Pb^{2+} and oxygen-containing active functional groups (such as C–OH and –COOH) or C=C (pi-electron) bonds.[40] Moreover, the adsorption capacity of SMA is compared with other reported adsorbents in the literature (Table S6†), indicating that the maximum adsorption capacity of the SMA resin (106.5 mg g^{-1}) for Pb^{2+} ions is favorable.

3.9 Desorption and reusability

To make the adsorption process cheaper and more feasible, the recovery and reusability of the SMA resin prepared from PJ seeds were explored (Fig. 10). The results show that 90.7% recovery is obtained at pH 2.5; this is because the adsorbent surface is protonated by hydronium (H_3O^+) ions when in an acidic state, making the desorption of Pb^{2+} ions from the SMA surface conceivable. To confirm the reusability of the SMA adsorbent, adsorption–desorption cycles were carried out multiple times utilizing the same adsorbent.

Fig. 11 shows the adsorption efficacy of SMA for Pb^{2+} ions over more than six progressive adsorption–desorption cycles. The obtained results revealed that the adsorption efficacy for Pb^{2+} ions diminished upon expanding the number of adsorption–desorption cycles, and toward the end of the sixth cycle, 86.3% adsorption efficacy was discovered for Pb^{2+} ions. The adsorbent was regenerated, but subsequent cycles showed lower removal percentages. The blocked pores of the SMA ion-exchange resin were effectively cleared by the desorbing agent. However, after completing the desorbing process, the SMA resin has an adsorption capacity that is comparatively lower than fresh SMA resin, owing to regeneration of Pb^{2+} ions from SMA. From this, SMA was seen to be a decent eco-friendly adsorbent and it could be successfully utilized for the removal of Pb^{2+} from water and wastewater.

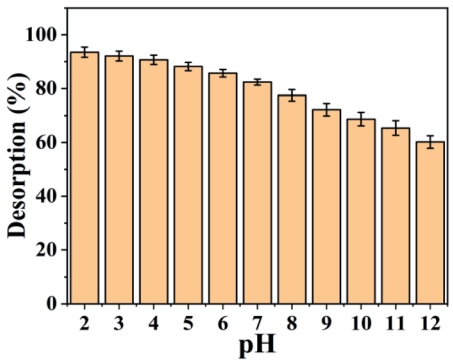

Fig. 10 The desorption percentages of the SMA resin at various pH levels.

3.10 DFT studies of the SMA ion-exchange resin

For computational calculations of the interactions of the SMA resin with Pb^{2+} ions, density functional theory (DFT) was selected due to its accuracy and unbiased computational competence.[46] The DFT studies were carried out using Gaussian 9 software. The Becke, 3-parameter, Lee–Yang–Parr (B3LYP) method was used with Los Alamos National Laboratory 2 Double-Zeta (LANL2DZ) as a basis set. To determine the adsorption characteristics of the resin, a four-membered fused pyrene ring was chosen to represent the molecular structure of the SMA resin. The pyrene ring with different functional groups was taken as the base structure for the interaction of the functional groups with Pb^{2+}. The functional groups that were considered in this work are –CHO, –C=O, –COOH, –SH, and an aromatic pi system. IR spectral results were considered for the selection of the functional groups based on the characterized absorption peaks. For Pb, the most common oxidation state of +2 in the singlet and triplet states (excited) was used to determine the energies of interaction between the ion and various functional groups. The binding energies (BEs) between the various functional groups and Pb^{2+} ions were calculated using the given formula:

$$BE_{Pb(II)-pyr} = E_{(pyr+functional\ group\ (Fg))} + E_{(Pb(II)\ in\ singlet\ or\ triplet\ state)} - E_{(Pb(II)\ in\ singlet\ or\ triplet\ state—pyr+Fg)}$$

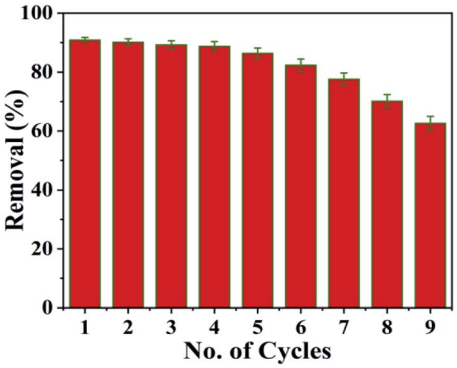

Fig. 11 The removal percentages of SMA resin for a number of adsorption process cycles.

 © 2021 The Author(s). Published by the Royal Society of Chemistry

Open Access Article. Published on 22 January 2021. Downloaded on 12/30/2025 1:39:20 AM.
This article is licensed under a Creative Commons Attribution-NonCommercial 3.0 Unported Licence.

The results from the computational study of the adsorption of Pb^{2+} ions onto the resin are given in Table S5.† In Table S5,† the BEs of Pb^{2+} ions with various functional groups and the bond distances between the functional groups and the Pb^{2+} ions can be seen. The presence of functional groups and their interactions with Pb^{2+} ions were determined *via* FT-IR spectroscopy. It can be seen from the IR data in Table S1† that the functional group peaks were shifted due to interactions between the heteroatoms of the functional groups and Pb^{2+} ions. Fig. 12a–d shows the optimized configurations of Pb^{2+} ions when interacting with the functional groups present in SMA. The five functional groups, namely an aromatic pi system and carbaldehyde, –C═O, –COOH, and –SH groups, were confirmed based on IR studies. Therefore, these functional groups were used for DFT calculations, and the optimized structures of the pyrene ring system with a functional group interacting with the metal are shown in Fig. 12e and f. The results of DFT analysis showed that the bond distances between the Pb^{2+} ion and the O atoms of the carbaldehyde, –C═O, and –OH groups were fairly constant, with a bond length of 3.30 Å. The chelating nature of carboxylic acid shortens the bond length between O and Pb^{2+} for both C═O and OH, but the resultant energies were found to be far lower compared with the other interactions (except for the SH and pi-interactions), suggesting that the chelating action of COOH provides less stabilization during the adsorption of Pb^{2+}.

The BE values suggest that Pb^{2+} ions in the triplet state show a better adsorption capacity than the singlet state for all functional groups. The aromatic ring pi-interaction with Pb^{2+} ions shows the lowest BE, suggesting that the attraction of Pb^{2+} ions to the aromatic ring was weak. However, the presence of a large number of such groups in the SMA resin makes the attraction between pi-electrons and Pb^{2+} ions important. The –SH group showed the next lowest BE towards Pb^{2+} ions. The size of sulfur and its less electronegative nature are responsible for the longer bond length and lower BE. The –COOH group show a lower BE towards lead due to the redistribution of electrons between CO and OH in the presence of Pb^{2+}. The singlet Pb^{2+}-ion ketonic group showed the highest BE compared to any other form, but for triplet Pb^{2+} ions, aldehyde and hydroxyl oxygen showed the highest BEs. The BEs of –CO and –OH were found to be nearly 328 kcal mol^{-1}, suggesting that moderate chemical adsorption may be involved in the mechanism of the adsorption of Pb^{2+} onto the SMA resin.

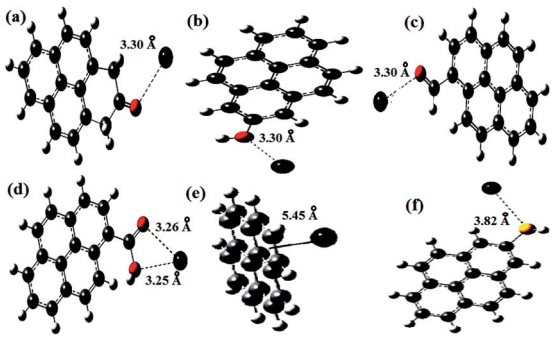

Fig. 12 The optimized configuration of a Pb^{2+} ion interacting with the functional groups present in SMA (a–d), and DFT calculations and the optimized structures of the pyrene ring system with functional groups interacting with a Pb^{2+} ion (e and f).

4. Conclusions

In summary, we have demonstrated that the inexpensive and eco-friendly adsorbent SMA resin has a significant adsorption capacity (106.5 mg g^{-1}) compared with other adsorbents reported in the literature (Table S6†) for the removal of lead ions from wastewater. The SMA resin revealed highly efficient Pb^{2+} removal (73.45% at pH 6), and chemical adsorption was favorable at higher temperatures. Moreover, the SMA resin indicates adsorption isotherm correlation in the following order: Langmuir > Freundlich > Koble–Corrigan > Temkin > Dubinin–Radushkevich. Kinetics studies indicate that the adsorption shows the best fit with pseudo-second-order kinetics, followed by pseudo-first-order and first-order kinetics. Thermodynamic studies showed that adsorption was spontaneous at all temperatures. An investigation of desorption and recovery revealed that HCl could be used as a desorption agent, and it gave desorption of 90.7% at pH 2.5; a removal percentage of 86.3% could be maintained for up to six cycles. The straightforward strategy used for the preparation of the SMA adsorbent, the minimal energy required, and the high removal capacity over a number of cycles support the use of this SMA adsorbent. DFT studies proved that the pyrene ring system with functional groups interacted with Pb^{2+}, and the proposed SMA resin showed high binding energies toward Pb^{2+}. Hence, these results highlight the advantages of this material for wastewater treatment for environmental applications.

Conflicts of interest

There are no conflicts to declare.

Acknowledgements

SA gratefully acknowledges the All India Council for Technical Education (AICTE) and Govt. College of Engineering, Salem-636011 (Tamil Nadu, India) for providing funding under the Technical Education Quality Improvement Programme (TEQIP) phase-III scholarship scheme.

Notes and references

1 Y. A. Yahaya, M. M. Don and S. Bhatia, *J. Hazard. Mater.*, 2009, **161**, 189–195.
2 A. Azimi, A. Azari, M. Rezakazemi and M. Ansarpour, *ChemBioEng Rev.*, 2017, **4**, 37–59.
3 T. Zehra, L. B. L. Lim and N. Priyantha, *Environ. Earth Sci.*, 2015, **74**, 2541–25514.
4 P. X. Sheng, Y. P. Ting, J. P. Chen and L. Hong, *J. Colloid Interface Sci.*, 2004, **275**, 131–141.

Open Access Article. Published on 22 January 2021. Downloaded on 12/30/2025 1:39:20 AM.
This article is licensed under a Creative Commons Attribution-NonCommercial 3.0 Unported Licence.

5 S. Lata, P. K. Singh and S. R. Samadder, *Int. J. Environ. Sci. Technol.*, 2015, **12**, 1461–1478.
6 C. Saka, Ö. Şahin and M. M. Küçük, *Environ. Sci. Technol.*, 2012, **9**(2), 379–394.
7 M. R. Lasheen, I. Y. El-Sherif, S. T. El-Wakeel, D. Y. Sabry and M. F. El-Shahat, *J. Mater. Environ. Sci.*, 2017, **8**, 503–511.
8 Y. Yu, J. Wang, J. Chen, X. He, Y. Wang, K. Song and Z. Xie, *J. Environ. Sci.*, 2016, **47**, 100–108.
9 S. Saber-Samandari, S. Saber-Samandari, N. Nezafati and K. Yahya, *J. Environ. Manage.*, 2014, **146**, 481–490.
10 A. Kaur and S. Sharma, *Indian J. Sci. Technol.*, 2017, **10**, 1–14.
11 S. Pap, J. Radonić, S. Trifunović, D. Adamović, I. Mihajlović, M. Vojinović Miloradov and M. Turk Sekulić, *J. Environ. Manage.*, 2016, **184**, 297–306.
12 K. Nuithitikul, R. Phromrak and W. Saengngoen, *Sci. Rep.*, 2020, **10**(1), 1–14.
13 J. Feng, J. Zhang, W. Song, J. Liu and Z. Hu, *Ecotoxicol. Environ. Saf.*, 2020, **203**, 111002.
14 S. H. Lin and R. S. Juang, *J. Environ. Manage.*, 2009, **90**, 1336–1349.
15 F. Mateen, I. Javed, U. Rafique, N. Tabassum, M. Sarfraz, S. Z. Safi, I. Yusoff and M. A. Ashraf, *Desalin. Water Treat.*, 2015, **14**, 1–9.
16 M. Carmona, A. De Lucas, J. L. Valverde, B. Velasco and J. F. Rodriguez, *Chem. Eng. J.*, 2006, **117**(2), 155–160.
17 K. Matsusaki, N. Hashimoto, N. Kuroki and T. Sata, *Anal. Sci.*, 1997, **13**(3), 345–349.
18 A. W. Trochimczuk, *Eur. Polym. J.*, 1998, **34**(7), 1047–1051.
19 S. Kobayashi, T. Tanabe, T. Saegusa and F. Mashio, *Polym. Bull.*, 1986, **15**(1), 7–12.
20 S. Raghav and D. Kumar, *J. Chem. Eng. Data*, 2018, **63**(5), 1682–1697.
21 M. Naushad, S. Vasudevan, G. Sharma, A. Kumar and Z. A. Alothman, *Desalin. Water Treat.*, 2016, **57**, 18551–18559.
22 X. Li and L. Yan, *RSC Adv.*, 2019, **9**(22), 12732–12736.
23 Y. Cheng, C. Yang, H. He, G. Zeng, K. Zhao and Z. Yan, *J. Environ. Eng.*, 2016, **142**, C4015001.
24 T. Qiu, J. Yang, X. Bai and Y. Wang, *RSC Adv.*, 2019, **9**, 12737–12746.
25 H. Bhunia and P. K. Bajpai, *RSC Adv.*, 2015, **5**(58), 46568–46582.
26 A. Sivaprakasam, T. Venugopal and K. Kannan, *Iran. J. Chem. Chem. Eng.*, 2020, **39**(6), 75–93.
27 Q. Li, Y. C. Lin, X. Chen and N. Yun, *J. Hazard. Mater.*, 2007, **148**(3), 671–678.
28 G. B. Adebayo, N. Abdus-salam and S. A. Elelu, *Ilorin J. Sci.*, 2014, **1**(1), 1–10.
29 T. Mutiara, F. I. Muhandi, A. Alhumaini, A. Chafidz and P. Hidayat, *Mater. Sci. Forum*, 2020, **981**, 331–335.
30 M. M. Habtegebrel and M. A. Khan, *Mod. Chem.*, 2018, **6**, 6–14.
31 S. H. Tabatabaei, M. Asemanrafat and M. Nousahdi, *E3S Web Conf.*, 2013, **1**, 13010.
32 K. C. Nebaghe, Y. El Boundati, K. Ziat, A. Naji, L. Rghioui and M. Saidi, *Fluid Phase Equilib.*, 2016, **430**, 188–194.
33 M. Imamoglu and O. Tekir, *Desalination*, 2008, **228**, 108–113.
34 C. K. Singh, J. N. Sahu, K. K. Mahalik, C. R. Mohanty, B. R. Mohan and B. C. Meikap, *J. Hazard. Mater.*, 2008, **153**, 221–228.
35 H. Wang and P. Luo, *Water, Air, Soil Pollut.*, 2020, **231**(7), 1–5.
36 G. Abimbola, Z. Zaman and P. Adeniyi, *J. Cleaner Prod.*, 2017, **148**, 958–968.
37 N. Gopal, M. Asaithambi, P. Sivakumar and V. Sivakumar, *J. Water Process. Eng.*, 2014, **2**, 87–95.
38 K. S. Obayomi, M. Auta and A. S. Kovo, *Desalin. Water Treat.*, 2020, **181**, 376–384.
39 Y. Huang, C. Yang, Z. Sun, G. Zeng and H. He, *RSC Adv.*, 2015, **5**, 11475–11484.
40 J. Zhang, J. Shao, Q. Jin, X. Zhang, H. Yang, Y. Chen, S. Zhang and H. Chen, *Sci. Total Environ.*, 2020, **716**, 1–9.
41 N. Gopal, M. Asaithambi, P. Sivakumar and V. Sivakumar, *J. Water Process. Eng.*, 2014, **2**, 87–95.
42 F. Batool, J. Akbar, S. Iqbal, S. Noreen, S. Nasir and A. Bukhari, *Bioinorg. Chem. Appl.*, 2018, **3**, 230–239.
43 Z. B. Bouabidi, M. H. El-naas, D. Cortes and G. Mckay, *Chem. Eng. J.*, 2018, **334**, 837–844.
44 H. Fan, X. Sun, Z. Zhang and W. Li, *J. Chem. Eng. Data*, 2014, **59**(6), 2106–2114.
45 A. A. Inyinbor and F. A. A. G. A. Olatunji, *Appl. Water Sci.*, 2017, **7**, 2297–2307.
46 A. Jellibi, I. Chaabane and K. Guidara, *Phys. E*, 2016, **84**, 1–9.

 © 2021 The Author(s). Published by the Royal Society of Chemistry